

# RESULTS FROM THE INITIAL OPERATIONS OF THE SNS FRONT END AND DRIFT TUBE LINAC\*

A. Aleksandrov for SNS collaboration, ORNL, Oak Ridge, TN 37830 USA

## Abstract

The Spallation Neutron Source accelerator systems will deliver a 1 GeV, 1.44 MW proton beam to a liquid mercury target for neutron scattering research. The accelerator complex consists of an H<sup>-</sup> injector, capable of producing one-ms-long pulses at 60 Hz repetition rate with 38 mA peak current, a 1 GeV linear accelerator, an accumulator ring, and associated transport lines. The 2.5 MeV beam from the Front End is accelerated to 86 MeV in a Drift Tube Linac, then to 185 MeV in a Coupled-Cavity Linac and then to 1 GeV in a Superconducting Linac. The staged beam commissioning of the accelerator complex is proceeding as component installation progresses. The Front End and Drift Tube Linac tanks 1-3 have been commissioned at ORNL. The primary design goals of peak current, transverse emittance and beam energy have been achieved. Beam with 38 mA peak beam current, 1 msec beam pulse length and 1 mA average beam current have been accelerated through the DTL tank 1. Results and status of the beam commissioning program will be presented.

## INTRODUCTION

The Spallation Neutron Source accelerator complex will provide a 1 GeV, 1.44 MW proton beam to a liquid mercury target for neutron production. The accelerator complex consists of an H<sup>-</sup> injector, capable of producing one-ms-long pulses at 60 Hz repetition rate with 38 mA peak current, a 1 GeV linear accelerator, an accumulator ring, and associated transport lines. The SNS accelerator systems are comprehensively discussed elsewhere [1]. The baseline linac beam has a 1 msec pulse length, 38 mA peak current, is chopped with a 68% beam-on duty factor and repetition rate of 60 Hz to produce 1.6 mA average current. The staged beam commissioning of the accelerator complex is proceeding as component installation progresses. At this point, the H<sup>-</sup> injector (Front End) and Drift Tube Linac tanks 1, 2 and 3 (of 6) have been commissioned at ORNL. A summary of baseline design parameters and beam commissioning results is shown in Table 1.

## FRONT-END PERFORMANCE AND COMMISSIONING RESULTS

The front-end for the SNS accelerator systems is a 2.5 MeV injector consisting of the following major subsystems: the rf-driven H<sup>-</sup> source, the electrostatic low energy beam transport line (LEBT), a 402.5 MHz RFQ,

\* SNS is managed by UT-Battelle, LLC, under contract DE-AC05-00OR22725 for the U.S. Department of Energy. SNS is a partnership of six national laboratories: Argonne, Brookhaven, Jefferson, Lawrence Berkeley, Los Alamos and Oak Ridge.

the medium energy beam transport line (MEBT), a beam chopper system and a suite of diagnostic devices. The front-end is required to produce a 38 mA beam of 2.5 MeV energy at 6% duty factor. The 1 ms long H<sup>-</sup> macro-pulses are chopped at the revolution frequency of the accumulator ring (~1 MHz) into mini-pulses of 645 ns duration with 300 ns gaps. After construction and initial commissioning at LBNL the Front End was shipped to Oak Ridge in the summer of 2002, installed at the SNS site and re-commissioned using a dedicated beam stop. The Front End has been providing beam for commissioning the rest of the linac since then and more than 2000 hours of operation time have been accumulated so far.

Table 1. SNS design vs. achieved beam parameters

	Baseline Design or Goal	Achieved
MEBT peak current [mA]	38	52
DTL1 peak current [mA]	38	40
DTL1-3 peak current [mA]	38	38
DTL1 beam pulse length [msec]	1.0	1.0
DTL1 average current [mA]	1.6	1.05
MEBT horiz. emittance [ $\pi$ mm mrad (rms,norm)]	.27	< .3
MEBT vertical emittance [ $\pi$ mm mrad (rms,norm)]	.27	< .3
DTL1 horiz emittance [ $\pi$ mm mrad (rms,norm)]	0.3	0.30 (fit), 0.40
DTL1 vertical emittance [ $\pi$ mm mrad (rms,norm)]	0.3 (RMS)	0.21 (fit), 0.31 (RMS)
DTL1 beam duty factor	6.0%	3.9%
MEBT Beam Energy [MeV]	2.5	2.45 $\pm$ 0.010
DTL2 output energy [MeV]	22.89	22.94 $\pm$ 0.11

## Ion Source and LEBT Performance

Details of the ion source and LEBT design can be found in [2]. General performance of the ion source during commissioning is summarized in Fig.1, where operational current is shown for each day of the last commissioning run. Since there are no beam diagnostics in the ion source or LEBT, the beam current is measured in the MEBT after the RFQ. A maximum current of 51 mA was achieved, significantly exceeding the base line requirement of 38 mA. An R&D program on the ion-source hot spare stand [3] yielded a significant increase of the ion source

availability: starting at 85.6%, it increased to 92.4% in the second, and finally to 97.8% in the most recent DTL1-3 run.

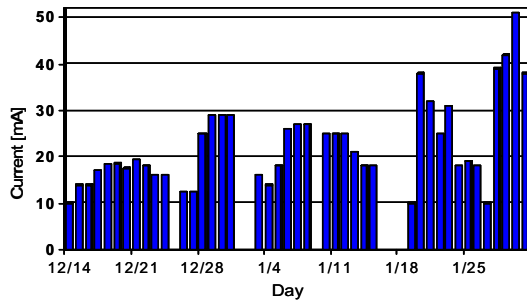


Figure 1: Peak beam current (average over 24 hours) at the MEBT exit for each commissioning day.

**RFQ Performance**

The design of the 3.72 m long 4-vane RFQ with p-mode stabilizers is described in detail elsewhere [4]. It operates at 402.5 MHz and accelerates H<sup>-</sup> beam from 65 kV to 2.5 MeV. Since the only tunable parameter for RFQ is the RF power, we used measurements of the RFQ transmission vs. RF power in order to establish the nominal set point. Since we couldn't measure the beam current injected into the RFQ from the LEBT, the absolute value of the RFQ transmission couldn't be calculated. Instead, we compared measured data with PARMTEQ simulations and derived the set point and expected transmission from the model, see Fig. 2.

The RFQ output energy was measured by a time-of-flight technique in the MEBT and found to be 2.45±0.01 MeV, compared with 2.50 MeV nominal design energy.

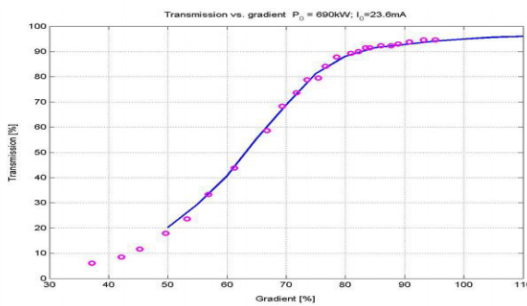


Figure 2: RFQ transmission vs. RF power. Measurements (red) and model fit (blue).

**MEBT Performance**

The MEBT is a complex beam transport line [5]. It matches the beam from the RFQ through the MEBT chopper system and into the drift-tube linac. Fourteen quadrupole magnets and four bunching cavities provide transverse and longitudinal focusing. The MEBT is equipped with a suite of beam diagnostics [6] including two beam current monitors (BCM), six beam position and phase monitors (BPM) installed within quadrupole magnets, and five dual-plane wire scanners (WS). A

temporary slit/collector type emittance device was installed at the MEBT exit for transverse emittance measurements during initial commissioning. It allowed measurements in one plane (vertical or horizontal). In order to switch to another plane vacuum had to be broken and the device physically rotated, therefore no simultaneous measurements in both directions were obtained. Typical emittance scan plots are shown in Fig.3.

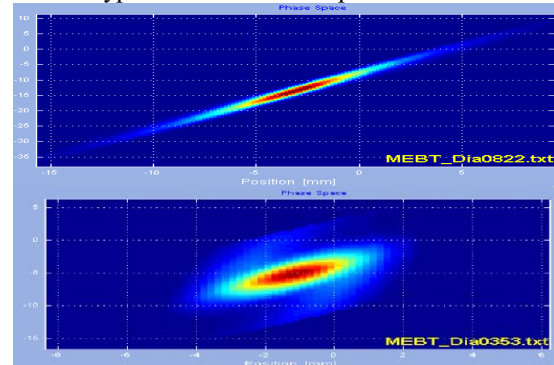


Figure 3: Typical beam vertical (upper) and horizontal (lower) transverse phase space measured at the MEBT exit.

The horizontal emittance scan in Fig. 3 clearly shows an S-shaped distortion caused by non-linear space charge forces. Even in the presence of the emittance growth due to non-linearity, the rms emittance values satisfy the requirements in a wide range of beam currents as illustrated in Fig. 4, where the output r.m.s. emittance is plotted vs. beam current.

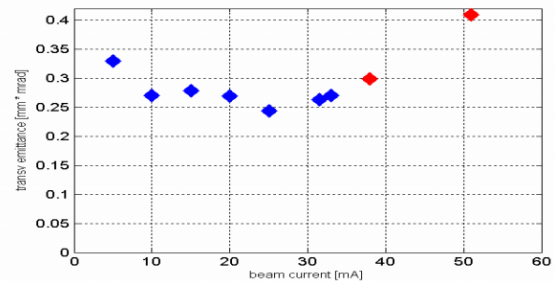


Figure 4: Transverse normalized rms emittance at the MEBT exit vs. beam current.

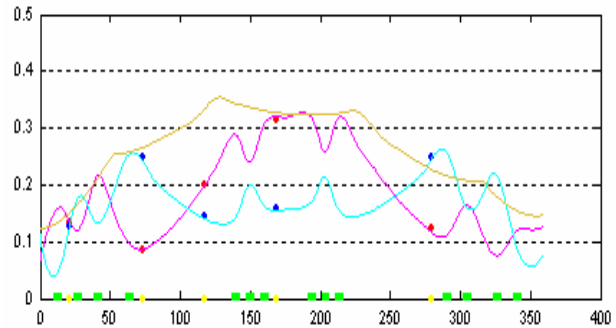


Figure 5: Beam profile (cm) vs. distance in the MEBT (cm). The points show measured horizontal and vertical beam profiles and the curves show the predicted horizontal profile (red), vertical profile (blue) and longitudinal profile (brown).

After proper tuning beam losses in the MEBT are below the measurement accuracy of the BCMs as illustrated by Fig. 7. In this picture the beam current pulse at the MEBT exit is shown on top of the beam pulse at the MEBT entrance.

Good understanding of the MEBT transverse optics was demonstrated. Figure 5 shows excellent agreement between measured horizontal and vertical beam profiles and those predicted from a model-based fit to the input Twiss parameters.

### Chopping

The 1 ms long H<sup>-</sup> macro-pulses have to be chopped at the revolution frequency of the accumulator ring into mini-pulses of 645 ns duration with 300 ns gaps. Beam chopping is performed by two separate chopper systems located in the LEBT and MEBT. The LEBT chopper removes most of the beam charge during the mini-pulse gaps, and the MEBT chopper further cleans the gap and reduces rise and fall time of the mini-pulse to 10 ns. The last lens in the LEBT is split into four quadrants to allow for electrostatic chopping using the RFQ entrance flange as a chopper target. The LEBT chopper system is complemented by a traveling-wave chopper in the MEBT that provides faster rise and fall times to 10 ns and further attenuates the beam in the gap to a level of 10<sup>-4</sup> [7]. Transient times of the gap produced by LEBT and MEBT choppers in the beam were measured using a BPM and fast oscilloscope - see Fig. 6 upper and lower signals respectively. The oscilloscope resolution did not allow an extinction ratio measurement to the design level of 10<sup>-4</sup>. Nevertheless, a laser based system capable of measuring rise/fall time with 5 ns resolution and beam extinction ratio with 10<sup>-4</sup> resolution was installed and tested but not with nominal chopped beam. Details can be found in [8].

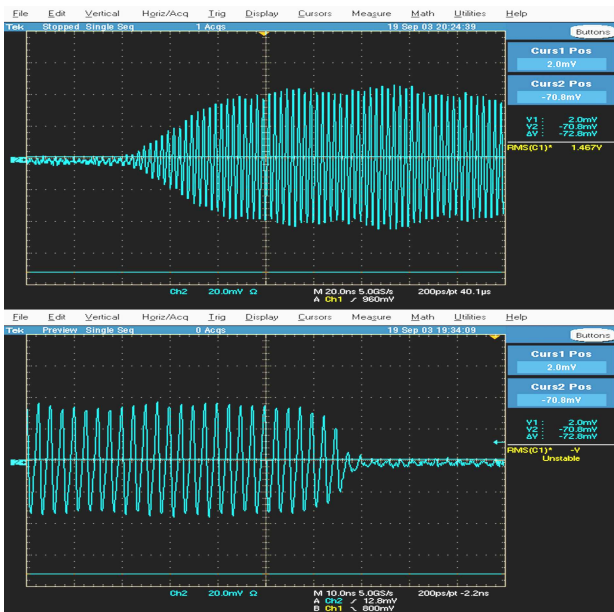


Figure 6: LEBT chopper rise time (upper trace) and MEBT chopper fall time (lower trace) measured at the MEBT exit.

## DRIFT TUBE LINAC PERFORMANCE AND COMMISSIONING RESULTS

The Drift Tube Linac consists of six accelerating tanks operating at 402.5 MHz with final output energy of 87 MeV. The transverse focusing is arranged in a FFODDO lattice utilizing permanent-magnet quadrupoles. Some empty drift tubes contain beam position monitors and dipole correctors. The intertank sections contain BCMs, wire scanners and energy degrader/faraday cups (ED/FC).

The first three of six DTL tanks have been commissioned with beam in two separate runs. The goals of the commissioning runs [9] have been to demonstrate full system functionality, demonstrate beam acceleration with design beam parameters to the limits of the available beamstop, test and validate beam commissioning algorithms, and commission the installed diagnostic devices.

### DTL Tank 1

In the first run, DTL tank 1 (with output energy 7.5 MeV) was commissioned into a dedicated Diagnostics System [10] (the “D-plate”) equipped with energy degrader/faraday cups, wire scanners, beam position monitors, a slit/harp emittance system, and a Bunch-Shape Monitor (BSM) [11], to enable detailed characterization of the output beam parameters, as well as a full-power beamstop for a test of high-power operation. DTL Tank 1 commissioning results are summarized in Table 1. The design peak current of 38 mA was readily achieved. A 1 msec long beam pulse was generated at 20 mA average current during the pulse (at low duty factor). Finally, a 1 mA average current beam was accelerated in DTL1 with 100% beam transmission. For this demonstration, a beam pulse of 26 mA peak current, 650 microsecond pulse length at 60 Hz (7.6 kW beam power) was achieved. Figure 7 shows an overlay of Beam Current Monitor signals in the MEBT and DTL1 during this high-power demonstration run. This was an important milestone, in that it shows the injector is capable of 1 MW-class SNS operation.

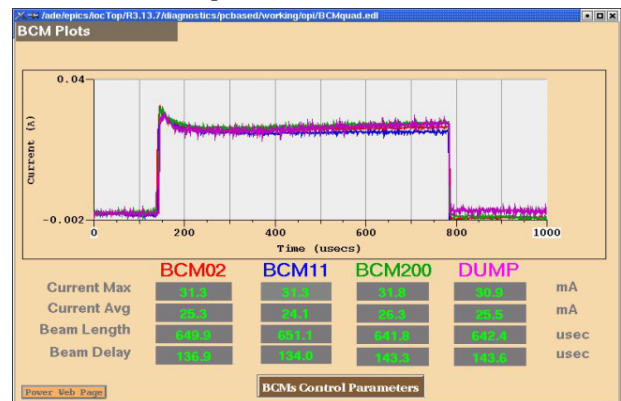


Figure 7: Beam current monitor traces during the DTL1 high-power run. The traces show the beam current after the RFQ (red), after the MEBT (blue), after DTL1 (green) and at the beamstop (purple).

The basic procedure for setting the RF phase and amplitude of the DTL tanks relies on the acceptance scan method utilizing the ED/FC located after each tank. The degrader thickness is chosen to absorb beam particles with energy just below the nominal acceptance. The phase and amplitude are determined by comparing the phase profile of the transmitted current with beam dynamics simulations. An example measurement is shown in Figure 8.

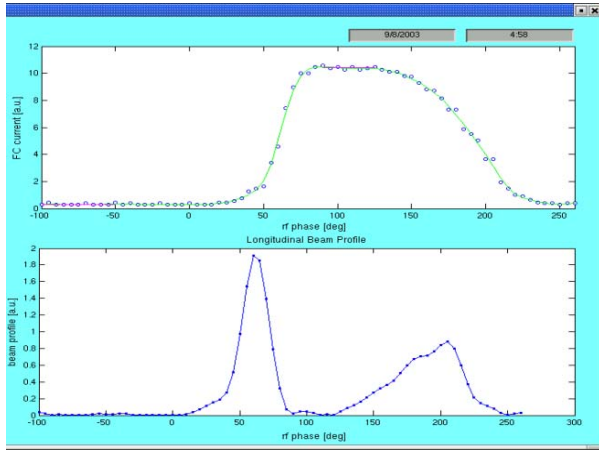


Figure 8: DTL tank 1 acceptance scan. The top curve shows the transmitted current through the degrader measured on the Faraday cup as a function of DTL1 phase. The lower curve is the derivative of the upper curve.

Extensive DTL1 output beam emittance measurements were performed with a slit-collector system. Figure 9 shows a horizontal emittance measurement at 38 mA peak current.

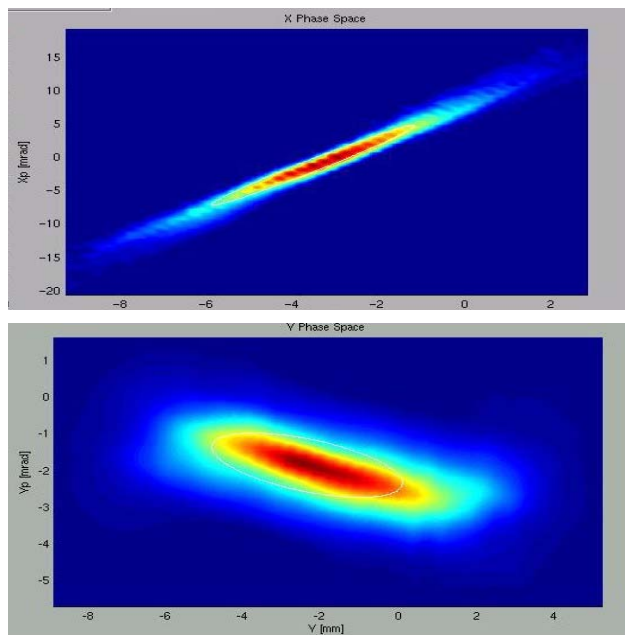


Figure 9: Horizontal (upper) and vertical (lower) output beam emittance from DTL tank 1 at 38 mA peak current. Angle (mrad) is plotted vs. position (mm).

The data are analysed in two ways. First, a Gaussian fit is performed to the two-dimensional beam distribution in position-angle space to obtain an emittance that can be considered representative of the beam core. Values obtained in this way are  $0.21 \pi$  mm mrad (rms, normalized) in the vertical plane and  $0.30 \pi$  mm mrad in the horizontal plane at 38 mA peak current, both of which achieve the emittance goal. In a second analysis, the RMS of the beam distribution is calculated with a 1% threshold (relative to the peak beam intensity) to remove spurious noise. Values obtained in this way are somewhat larger than the core emittances:  $0.31 \pi$  mm mrad, and  $0.40 \pi$  mm mrad in the vertical and horizontal respectively. A number of systematic effects in the emittance data are being investigated. For example, we see evidence of a large slit-scattering component that produces an opposite-sign signal (since the H<sup>-</sup> ion is stripped to protons) which reduces the beam signal. Analysis and modelling of slit-scattering and its correction is underway. We also observed a discrepancy between emittance device and wire scanner measurements in the horizontal plane, which is under investigation.

A number of measurements pertaining to the longitudinal dynamics were obtained from BSM measurements and will be discussed in a separate publication [11].

### DTL Tanks 2 and 3

In a third commissioning run, DTL Tanks 1-3, with output energy of 40 MeV, were commissioned into a low-power beam stop. Again, a peak current of 38 mA was readily transported through all three tanks with 100% transmission (within the 2-4% BCM measurement uncertainty). The beamstop limited pulse lengths to less than 50 microseconds, and repetition rates to 1 Hz. It is notable that the trajectory errors with all dipole correctors turned off remains within  $\pm 1.5$  mm in the MEBT/DTL1-3 system. Correction of the trajectory makes no measurable improvement in beam transmission.

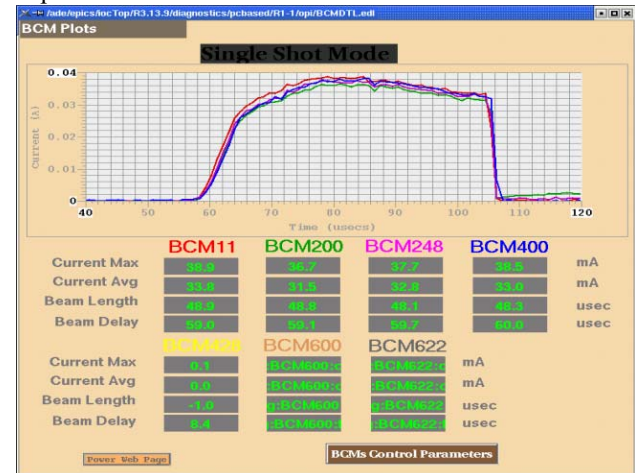


Figure 10: Beam current monitor traces during the DTL1-3 run. The traces show the beam current after the MEFT (red), after DTL1 (green), after DTL2 (purple) and after DTL3 (blue).

A second technique for determining DTL tank phase and amplitude setpoints, as well as determining the input energy, was explored. In this method, based on the “phase-scan signature matching” approach [12], the beam phase from a single BPM, or the phase difference between two BPMs downstream of a DTL tank, are measured as a function of the tank phase and amplitude.

Figure 10 shows an example for DTL1, in which three sets of measured phase differences were recorded from BPMs located after DTL tank 1. The data are limited only to those points where more than 7 mA of beam current was transported in order to ensure a reliable beam phase measurement. One scan was taken at nominal RF amplitude, one at 5% above nominal, and the other at 5% below nominal. As is evident in the figure, the signatures are quite sensitive to the RF amplitude. A model-based fit was then performed to these three phase-scan “signatures” to obtain the RF amplitude, relative phase of beam and RF, and the input energy. Interestingly, the input energy of 2.45 MeV, measured in this way, agrees with that measured by TOF in the MEBT. This is a powerful method that promises to offer more accurate determination of DTL setpoints than the acceptance scan method utilizing an ED/FC.

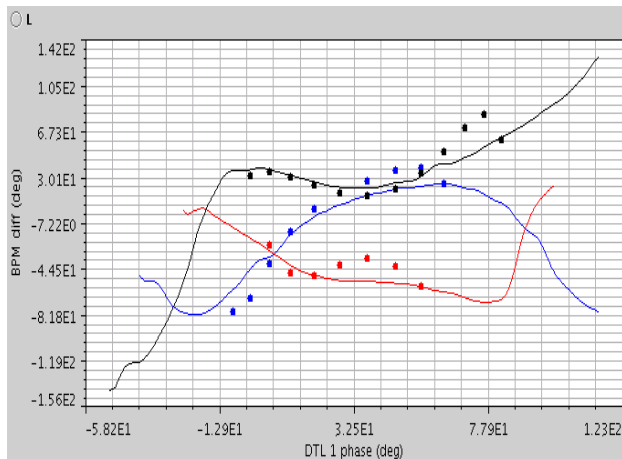


Figure 11: Curves show the measured phase difference (degrees) between two BPMs downstream of DTL1 as functions of DTL1 RF phase for nominal RF amplitude (blue), 5% below nominal (red) and 5% above nominal (black). The points show the result of a model-based fit to the data.

Time-of-flight measurements were also performed. Using BPMs located in DTL3 with the tank unpowered, a DTL2 output energy of  $22.94 \pm 0.11$  MeV was measured, which agrees with the design value within measurement uncertainty. The energy jitter and long-term drift were also measured. Averaging all data taken during a 30-minute period results in 0.08% rms output energy stability, which corresponds to 0.6 degree phase stability measured on a single BPM.

### OPERATIONAL STATISTICS

One of the important results of the commissioning activity is the improvement of the hardware reliability. A

summary of operational statistics for all three commissioning runs is shown in Table 2. Beam availability has been steadily improving despite an increase in the number of hardware systems under commissioning in each run, and reached 75% during the DTL1-3 commissioning run.

Table 2. Operational statistics

	Run 3 (DTL1-3)	Run2 (DTL1)	Run1 (FE)
Total time [hours]	288	1136	800
Beam available [%]	75	62	53
Planned shutdown [%]	6	2	2
Equipment breakdown[%]	19	36	45
Breakdown statistics by equipment group [%]			
RF	15	28	34
Power supplies	0	22	4
Ion Source	6	21	32
Diagnostics	0	6	7
Controls	4	17	12
Water, vacuum, etc.	75	6	11

### CONCLUSIONS

Commissioning of the SNS linac has been progressing well. Acceleration to 40 MeV of beam pulses with the peak design current of 38 mA has been readily achieved. The Front End and DTL1 were operated at 1 mA average current. Beam availability increases steadily with each commissioning run.

The remaining DTL tanks 4-6 and CCL have been installed in the tunnel and RF processed to the nominal power. They will be commissioned in the next commissioning period in fall 2004.

### REFERENCES

- [1] N. Holtkamp, Proc. PAC 2003, p. 11.
- [2] R. Keller et al., in "9th Int. Symp. on the Production and Neutralization of Negative Ions and Beams", edited by M. Stockli, AIP Conf. Proc. No. 639, p. 47.
- [3] R. Welton et al, Proc. PAC 2004.
- [4] A. Ratti et al., Proc. EPAC 2000, p. 495.
- [5] J. Staples et al., Proc. LINAC 2000, p. 250.
- [6] S. Assadi, Proc. PAC 2003, p. 498.
- [7] R. Hardekopf et al., PAC 2004.
- [8] A. Aleksandrov et al., PAC 2003, p. 1524.
- [9] E. Tanke et al., Proc. LINAC 2002, p. 353.
- [10] M. Plum et al., Proc. PAC 2001, p. 2374.
- [11] A. Feshenko et al., these proceedings.
- [12] T. Owens et al., Part. Acc. **48** (1994) p. 169.